PCCP

Accepted Manuscript

ROYAL SOCIETY OF CHEMISTRY

www.rsc.org/pccp

PCCP

RSCPublishing

ARTICLE

A comparison of homopolymer and block copolymer structure in 6FDA-based polyimides

Cite this: DOI: 10.1039/xoxxoooooox

I. Tanis [a*], D. Brown [a*], S. J. Neyertz [a], R. Heck [b] and R. Mercier [b]

Received ooth January 2012,
Accepted ooth January 2012

DOI: 10.1039/xoxxoooooox

www.rsc.org/

Two homopolyimides and the corresponding block copolyimide, all based on the 4,4'-(hexafluoroisopropylidene)diphthalic dianhydride (6FDA) have been synthesized and fully atomistic models have been studied using molecular dynamics (MD) simulation. The respective diamines were: 1,3-phenylenediamine (mPDA) and 2,3,5,6-tetramethyl-1,4-phenylenediamine (durene). These polyimides are potential candidates for gas separation applications. The synthesized polymers were processed as dense flat membranes. The effects of diamine structure were investigated at the molecular level and an attempt to compare the structural features of homo- and block copolyimides was performed. Amorphous models were generated using a hybrid pivot Monte Carlo-MD sampling preparation technique. Average model densities were validated against experimental measurements on the dense films. Cohesive energies, Hildebrand solubility parameters, conformational characteristics, intermolecular interactions and available void spaces were analysed for each system. The durene diamine was found to hinder stacking and increase the available space. This is associated to the steric effect of the methyl substituents. In general, 6FDA-mPDA/durene exhibits an intermediate behaviour with respect to its base polyimides. For most of the examined properties, the differences between different size simulated systems were minor with the exception of the free volume distribution.

1. Introduction

Aromatic polyimides have come forth as a promising family of polymers for a wide range of industrial applications [1-8]. At the first stage of their synthesis, a diamine reacts with a dianhydride in an aprotic solvent and yields a polyamic acid. This polymer undergoes polycondensation (either thermally or chemically) to form the desired polyimide [9].

Presently, polyimides are well known for their excellent thermal and chemical stability, low dielectric constant, and high radiation resistance [10]. These features render them attractive candidates in applications ranging from microelectronics [11], optics [12], radiation resistance [13] and aerospace engineering [14] to gas separation [15, 16]. A further improvement of their properties can be accomplished via chemical modification of the chain backbones and higher-order structure control [10].

The introduction of fluorine atoms into polyimides results in the production of materials with additional attractive features such as low water uptake, low permittivity, low refractive index and resistance to wear and abrasion [1]. Specifically, in the field of membrane gas separation, hexafluorodianhydride (6FDA)-based polyimides have gained special attention [17-23]. The substitution of CH_3 groups by CF_3 groups considerably increases the stiffness of the chain, allowing the membrane to separate molecules on the basis of steric bulk more effectively. Concurrently, chain packing is inhibited by the large CF_3 groups leading thus to an increase in permeability [22]. Finally, the imposed restriction of the intrasegmental mobility limits the distribution of gap sizes that are responsible for penetrant diffusion, thereby increasing diffusivity selectivity [3, 21]In view of the above reasons, 6FDA-based polyimides consistently deviate from the general relationship between permeability and permselectivity by showing systematically higher selectivities at values of permeability equivalent to other polymers [21, 24].

Most experimental efforts in the field of polyimides include thermal, mechanical and permeation analyses as well as density and solubility measurements [25]. Polyimides can also be examined via UV-visible spectrophotometry [26] and positron annihilation lifetime spectroscopy (PALS) [27]. Nonetheless, the synthesis of novel polyimides and associated laboratory analysis can often be time-consuming and economically demanding. Computational approaches, such as Molecular Dynamics (MD) simulation [28], can shed light on mechanisms

that operate at the molecular level [29,30] and therefore enhance and complement experimental efforts [31, 32]. The efficiency of computer simulations in polymers is largely dependent on the preparation of realistic starting structures [33]. Several methods for generating well-equilibrated polymer samples have been reported including modified rotational isomeric state (RIS) [34], in situ polymerization [35], continuum configurational bias Monte Carlo [36] as well as multi-scale techniques involving coarse-graining and reverse-mapping back to the atomistic scale [37, 38]. A number of simulation studies were directed towards the thermal and mechanical properties of polyimides [39-46] whereas several others have focused on structural and bulk characteristics [47-52]. However, to our knowledge, structural and void space features of block copolyimides have not been examined at the molecular level in contrast to their base homopolyimides.

In this work, structural aspects of three 6FDA-based polyimides with potential use in gas separations, are assessed via all-atom MD simulations and pertinent experiments. More specifically, we consider 2,2'-bis (3,4'dicarboxyphenyl) hexafluoropropane-1,3-phenylenediamine (6FDA-mPDA) which presents good-to-excellent selectivities for gas pairs of similar dimensions like N_2/CH_4 [53-57]. Additionally, we examine 2,2'-bis (3,4'dicarboxyphenyl) hexafluoropropane-2,3,5,6-tetramethyl-1,4-phenylenediamine (6FDA-durene) polyimide which, in contrast, yields very high permeabilities but low selectivities [53, 58, 59]. The advantages of these two homopolymers have been already combined to develop a random copolyimide (6FDA-mPDA/durene) [60, 61] with improved features for gas separation applications. In this study, properties of a 6FDA-mPDA/durene block copolyimide are assessed as well.

An earlier simulation approach addressed the effect of residual solvent on the free volume of 6FDA-mPDA polyimide [62] whereas Heuchel *et al.* evaluated transport properties of various gases in 6FDA-durene via the Gusev-Suter method [63]. In both studies the authors used the modified rotational isomeric state method to generate the atomistic models of the polyimides. In this procedure chains are grown into a simulation box where the density is gradually increasing. This has been known to lead to a bias in chain statistics [64]. This bias can eventually be relaxed out if there is sufficient chain flexibility and if the simulation time-scale is sufficiently long. This was not the case in both studies where only 50 ps of constant volume-constant temperature (NVT) [62] and 300 ps of constant isotropic pressure-constant temperature (NpT) MD [63] were used to relax the systems.

In this work, realistic amorphous models of the 6FDA-based polyimides have been generated through the use of a variant of the phantom chain growth approach [64, 65]. Experimental work involved the preparation of the corresponding dense films. Configurational and conformational properties are examined together with structural and void space attributes. Simulation results are confronted to experimental evidence from this work and other sources. The results of this study could aid in the design of polymer membranes with tailored permselectivity properties. Polymer synthesis and characterization are described in section 2 whereas simulation details are given in section 3.

2. Experimental

2.1 Materials

The homo- and copolyimides under study were prepared from 2,2'-bis(3,4'-dicarboxyphenyl)hexafluoropropane dianhydride (6FDA) (recrystallised from acetic anhydride), 2,3,5,6-tetramethyl-1,4-,phenylenediamine (durene diamine) (Aldrich), and 1,3-phenylenediamine (mPDA) (Aldrich).

2.2 General synthetic procedure for homopolymers

mPDA (10 mmol) was dissolved in m-Cresol (27.6 mL), 6FDA (10 mmol) was added and the mixture was stirred at 180 °C under N_2 for 8 hours. The reaction was cooled to room temperature and diluted with 10 mL m-Cresol. The mixture was poured into methanol (250 mL). The resulting polymer was filtered, washed with methanol, crushed and extracted with methanol (soxhlet) to remove any remaining trace of m-Cresol. The polymer was then dried at 150 °C under vacuum overnight.

6FDA-mPDA, 1H NMR (400 MHz, DMSO-d6, δ, ppm): 8.17 (d, 2H, 6FDA), 7.93 (d, 2H, 6FDA), 7.75 (s, 2H, 6FDA), 7.68 (t, 1H, mPDA), 7.55 (s, 1H, mPDA), 7.52 (d, 2H, mPDA). 6FDA-durene, 1H NMR (400 MHz, DMSO-d6, δ, ppm): 8.21 (d, 4H, 6FDA), 7.96 (s, 2H, 6FDA), 2.06 (s, 12H, CH3).

2.3 Synthetic procedure for 6FDA-mPDA/durene block copolymer

mPDA (10 mmol) was dissolved in *m*-Cresol (25 mL) under N_2, 6FDA (8.99 mmol) was added and the mixture was stirred at 180°C under N_2 for 8 hours. The reaction was cooled to room temperature. 6FDA (8.48 mmol), durene (7.47 mmol) and *m*-Cresol (25 mL) were added to the mixture and the reaction was stirred for 8 more hours at 180 °C under N_2. The reaction was cooled to room temperature, diluted with *m*-Cresol (20 mL) and poured into methanol (500 mL). The resulting polymer was filtered, washed with methanol, crushed and extracted with methanol (soxhlet) to remove any remaining trace of *m*-Cresol. The polymer was then dried at 150 °C under vacuum overnight. ^{1}H NMR (400 MHz, DMSO-d_6, d, ppm): 8.17 (d, 4H 6FDA), 7.95 (br, 4H 6FDA), 7.76 (br, 4H, 6FDA), 7.64 (m, 1H, mPDA), 7.55 (s, 1H, mPDA), 7.52 (br, 2H, mPDA), 2.05 (s, 12H, CH_3).

2.4 Characterization

Glass transition temperatures (T_g) were determined using a Metler Toledo DSC822^e differential scanning calorimeter with a heating rate of 10°C/min. Thermogravimetric analysis (TGA) was conducted using a TA instruments TGA Q50. The polymers were heated from 35°C to 700°C at 10°C/min.

Film density was determined on small squares of membranes by flotation with n-hexane and tetrachloroethane in

a thermostatic bath at 20°C. Number average molecular weights (M_n) were derived from Carothers' equation [66]. The synthetic pathway of the polyimides leads to a narrow distribution of M_w [67, 68]. Consequently, the polymer molecular weight estimation via Carothers' equation holds quite well.

2.5 Preparation of dense flat membranes

Dense films were prepared by a casting method. An N-methyl-2-pyrrolidone (NMP) solution containing about 20 wt% polymer was filtered through a 45-mm filter then a 10-mm filter and finally a 1-mm filter to remove nondissolved materials and dust particles. The solution was then cast on a clean glass plate using a casting ring. The whole plate was covered with a hood with a small gap to allow the solvent to slowly evaporate; a stream of nitrogen was passed through the hood. The plate was slowly heated for 24 hours following a preset heating sequence to allow for film formation. The resulting film was finally dried in a vacuum oven at 150°C overnight to remove residual solvent. The chemical structures of the polyimides are depicted in Figure 1.

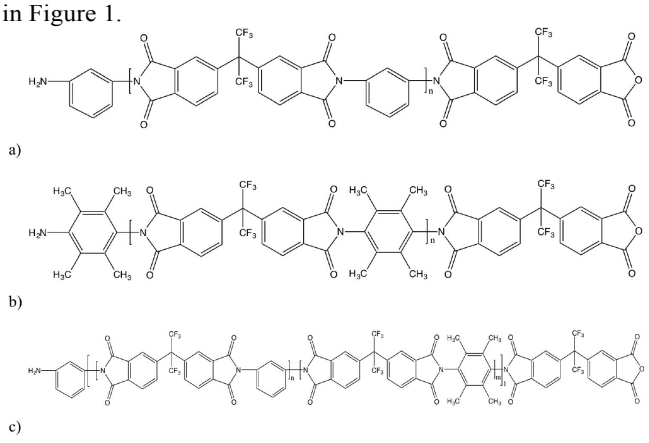

Figure 1. Schematic representation of the chemical structures of a) 6FDA-mPDA, b) 6FDA-durene and c) 6FDA-mPDA/durene.

3. Simulation protocol

3.1 Force-field

All MD simulations were conducted using the scalar and parallel versions of the *gmq* software [69, 70]. Interaction parameters for the polymers were obtained from the TRIPOS 5.2 force field [71] which has been successfully applied to a large number of cyclic compounds [72-78] and other types of polymers [43, 79, 80]. The actual functional form of the potential used in *gmq* is given by [70]

$$U_{pot} = \sum_{\theta} \frac{k_\theta}{2}(cos\theta - cos\theta_0)^2 + \sum_{\tau}\sum_{n=0}^{6} \alpha_n cos^n \tau + \sum_{i-sp^2} \frac{k_{oop}}{2} d^2 + \sum_{(i,j)_{nb}} 4\varepsilon_{ij}\left(\left(\frac{\sigma_{ij}}{|r_{ij}|}\right)^{12} - \left(\frac{\sigma_{ij}}{|r_{ij}|}\right)^{6}\right) + \sum_{(i,j)_{nb}} \frac{q_i q_j}{4\pi\varepsilon_0 |r_{ij}|} \quad (1)$$

where the first three terms describe the bending, torsional and out-of-plane contributions to the total potential energy whereas the two final terms represent the dispersive and coulombic energy respectively. Van der Waals interactions between atoms belonging to the same molecule (but separated by more than two bonds) as well as atoms belonging to different molecules are modelled by the Lennard-Jones (L-J) 12-6 potential. The ε_{ij} and σ_{ij} cross-terms were obtained from the geometric mean of ε_{ii} and ε_{jj} and from the arithmetic mean of σ_{ii} and σ_{jj}. All electrostatic interactions have been calculated via full Ewald summation [81]. As is common practice in such simulations, the high frequency low-amplitude bond stretching modes were removed by the SHAKE routine in order to avoid difficulties with the equipartition of kinetic energy[82]. In addition to simple bond constraints, the high frequency low amplitude modes associated with hydrogen atoms in CH_3 groups were also frozen out [82]. All bond lengths were rigidly constrained to standard values. This allowed to set the simulation time-step to 1 fs. Partial charges on the atoms were obtained by performing ab-initio calculations on representative three-fragment structures of the polyimides under study by utilizing Gaussian 03 [83] at the B3LYP/6-31G** level. Point charges were extracted for the central and end moieties of the model fragments by an electrostatic potential fitting (ESP) procedure [84] and are available as supplementary material.

3.2 Validation of the hybrid PMC-MD technique

Amorphous models of the polyimides under study were generated through the use of the well-established hybrid pivot Monte Carlo-Molecular dynamics (PMC-MD) technique [72-78]. This approach allows the polymer samples to be constructed at the desired density with conformations corresponding to the equilibrium melt at the required temperature. It involves a single-chain sampling procedure based on occasional pivot Monte Carlo moves for a certain number of pre-selected torsions at fixed intervals of a standard MD simulation. The latter is very efficient at sampling the oscillatory modes of a polymer molecule. The underlying theory originates from Flory's hypothesis according to which, the configurations of polymer chains in the pure melt are governed by only a certain number of near-neighbour intramolecular interactions [85, 86]. In other words, only interactions between atoms separated by no

more than a certain number of backbone bonds (n_{bonds}) are considered.

The method has been tested on various polymers with small chain lengths for which equilibrium can be achieved in reasonable MD time-scales. Comparison of the results for chains decorrelated through PMC-MD with those of a bulk melt system decorrelated using exclusively MD has, in most cases, shown excellent agreement [49, 50, 78, 87]. This suggests that PMC-MD, after being validated on oligomer samples, can provide well-equilibrated melt samples of molecules of arbitrary length.

The assessment of the method showed that, although for a large number of polymers n_{bonds} was found to be equal to 4, its value is not universal and therefore needs to be optimized for all three polyimides under study [85, 86]. This can be accomplished by comparing structural characteristics of chains sampled by the PMC-MD method with those of a fully interacting bulk melt system decorrelated by MD on its own [78]. Considering the high stiffness of polyimides, this comparison can only be achieved for short homologues at a temperature high enough to ensure decorrelation of the bulk melt.

To this end, single-chain systems of four monomers were relaxed through PMC-MD for a variety of n_{bonds} values at 1000 K. Sampling was carried out for a total time of 3000 ps during which torsional pivot moves were attempted every 100 time steps. Configurations were saved every 5 ps.

To create the corresponding bulk oligomer samples, for each polyimide system, 20 uncorrelated chains generated via the single-chain sampling procedure were randomly distributed in a cubic box and the full potential was afterwards switched on. The total number of atoms was equal to 4760 in the case of 6FDA-mPDA, 5960 for 6FDA-durene and 5240 for 6FDA-mPDA/durene copolyimide. The bulk melts were subjected to MD runs at the NpT ensemble at 1000 K in which the isotropic pressure was maintained at 1 bar by loose-coupling [88] to a barostat with a coupling constant of 5 ps and temperature [89] was held constant by coupling to a heat bath with a constant of 0.1 ps. The van der Waals potential was truncated at R_c = 10Å and long-range corrections to the energy and pressure were applied. The normalized autocorrelation function for the end-to-end vector of the individual chains was calculated in order to verify that the chains were decorrelated from their initial configurations.

$$C_R(t) = \frac{\langle R_i(0)R_i(t)\rangle - \langle R_i\rangle^2}{\langle R_i^2\rangle - \langle R_i\rangle^2} \quad (2)$$

Figure 2 displays the $C_R(t)$ for both single-chain and bulk melt 6FDA-durene systems using an n_{bonds} value of 4. It can been observed that decorrelation is achieved for both systems over the time scale considered. The PMC-MD sampled chain decorrelates within a few hundred ps whereas in the bulk melt system chains take ~7000 ps to fully decorrelate.

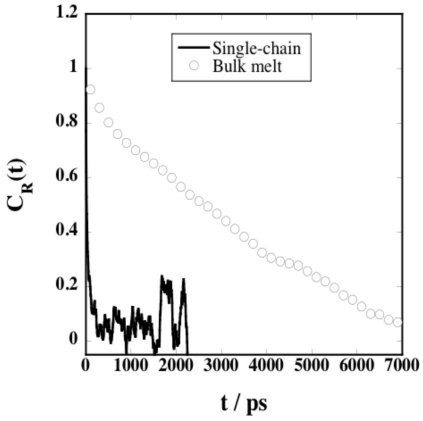

Figure 2. Normalized autocorrelation function for the end-to-end vectors, $C_R(t)$, of four-monomer 6FDA-durene chains, sampled both via PMC-MD (line) and with bulk melt MD (circles) at 1000K.

The autocorrelation functions of square end-to-end distances (not shown) also demonstrated the decorrelation of both single-chain and bulk melt samples. After verifying that both single-chain sampled and bulk systems were independent of their initial configurations, comparison of structural properties such as the probability densities of the mean-square end-to-end distances $\langle R^2\rangle$, the mean-square radii of gyration $\langle S^2\rangle$, and specific pivot torsional angles was performed. The distributions of $\langle R^2\rangle$ as well as those of the C-C-C-F pivot torsion angle (the angle that links the CF_3 groups in the 6FDA fragment) for the four-monomer 6FDA-mPDA system for n_{bonds} = 4 are depicted in figure 3.

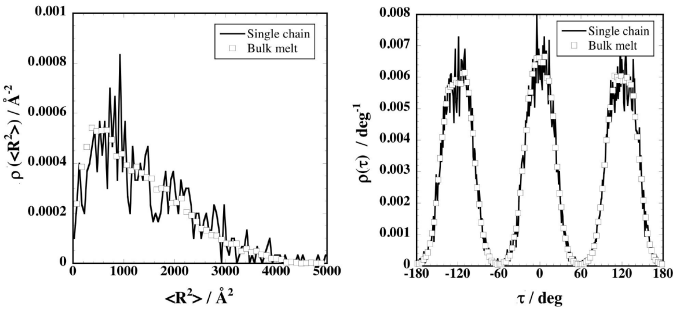

Figure 3. Probability densities for the square end-to-end distances (left) and the pivot C-C-C-F torsion angle (right) for 6FDA-mPDA four-monomer chains at 1000 K for n_{bonds} = 4. Results are compared for single-chain sampled systems and bulk oligomer melts.

It can be clearly seen from figure 3 that the distributions are superimposable for n_{bonds} = 4 unlike the results obtained for n_{bonds} = 3 (not shown). A similar level of agreement has been found in the distributions of the mean-square radii of gyration $\langle S^2\rangle$ and the C-C-C-C torsional angle which connects the rings in the 6FDA fragment for all polyimides. The previous results demonstrate that the hybrid PMC-MD method with a value of the local energy parameter equal to 4 is an efficient way to sample the configurations of short oligomers of the polyimides in melt conditions and we now use this value to generate initial

configurations for longer chain lengths. It is worth noting that the average radii of gyration were found to be in the order 6FDA-durene > 6FDA-mPDA/durene > 6FDA-mPDA, suggesting that 6FDA-durene oligomers are more extended than their counterparts.

3.3 Generation of the Amorphous Polyimide Models

Previous simulation studies in 6FDA-based polyimides considered various chain lengths in the PMC-MD single-chain sampling procedure and reported that the value of $\langle R^2 \rangle / n_{monomers}$ becomes number independent from $n_{monomers}$ ~30 [50, 90]. Taking also into account the average molecular weights of the synthesized polyimides, we generated amorphous models containing chains with a number of monomers equal to 88 for 6FDA-mPDA (8278 atoms), 79 for 6FDA-durene (9328 atoms) and 85 for 6FDA-mPDA/durene (8956 atoms). The latter consisted of 4 blocks with a monomer ratio of 11/10.

For all polyimide models, the required number of uncorrelated chains were generated via PMC-MD at a temperature close to or above the glass transition temperature of the respective polyimide. The generation temperature was set to 700 K for all polyimides since experimental measurements of their T_g (this work and other sources) range from 600 to 700 K [54, 56, 57, 60, 61, 91]. The chains were randomly distributed in a periodic cubic box. For each polyimide under study a two- and a five-chain system was built. Bearing in mind the high stiffness of the materials under study as well as the relatively short time scales of MD simulations in comparison to the relaxation times of glassy polymers, it was essential to avoid large scale volume fluctuations upon switching on the full potential. Hence, the box sizes were set to values close to the experimental density. Excluded volume was introduced progressively [78], by scaling the van der Waals potential by a factor varying linearly from 0 to 1 over a period of 10 ps under NVT conditions. To preclude unphysical trapping of bonds in the rings as the intermolecular interactions are switched on, "phantom" atoms with the mass of a carbon were placed at the center of each ring. Following the activation of the van der Waals interactions, these phantom atoms were removed and coulombic interactions were switched on. The optimal parameters [92] of the Ewald sum were : $\alpha = 0.25$ Å^{-1} (6FDA-mPDA), 0.24 Å^{-1} (6FDA-durene and 6FDA-mPDA/durene); $K_{max} = 16$ (6FDA-mPDA) and 15 for 6FDA-durene and 6FDA-mPDA/durene copolyimide; the real space truncation radius R_c was set to 10 Å for all systems. The van der Waals truncation radius was also set to 10 Å for all systems and standard long-range corrections to the energy and pressure were made for interactions exceeding the truncation radius.

The systems were then heated to 1000 K in an attempt to relieve any remaining local steric hindrances. It has to be understood that there is no attempt to equilibrate the long chains in a liquid state at this higher temperature. This would not be appropriate. The chains are prepared with conformations corresponding to the equilibrium liquid state at a temperature close to the *experimental* glass transition temperature (700 K) using the hybrid PMC-MD technique. This is the temperature where at experimental cooling rates the polymer chains fall out of equilibrium. On the MD time scale, heating to even 1000 K does not lead to significant changes in the overall conformations of these relatively stiff chains which are thus preserved close to those required. It does, however, lead to local relaxations which can influence chain packing. Constant volume-constant temperature dynamics were thus performed at the elevated temperature for 500 ps before gradual cooling to room temperature (298 K) at a rate of -0.1 K/ps. This cooling rate is at least 10 orders of magnitude higher than corresponding experimental values but similar to typical cooling rates reported in simulation literature[40, 44, 93, 94]. However, the choice of the the experimental glass transition temperature (700 K), i.e. that pertinent for typical laboratory cooling rates, for the preparation of the chain conformations leads to the closest correspondence to experiment that can be reasonably achieved with current computing resources. A short NVT relaxation then followed before switching to isobaric-isothermal (NPT) conditions. At the final stage of the simulation protocol, the box was allowed to relax towards its equilibrium size and density by loose coupling using a coupling constant of 5 ps. Production runs were then carried out up to at least 4 ns with a time-step of 1 fs and frame-saving frequency of 10 ps. Figure 4 displays a snapshot of the equilibrated 6FDA-mPDA system using the VMD 1.9 software [95].

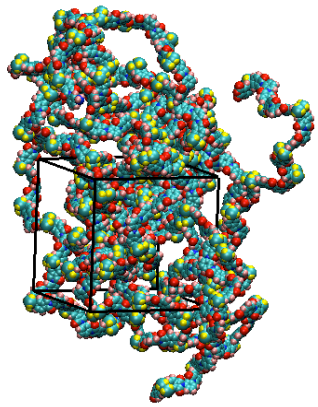

Figure 4. Schematic representation of the 2-chain 6FDA-mPDA simulation box displaying the primary ("unfolded") positions of polymer atoms (color code: yellow = F, red= O, cyan = C, blue = N, pink = H).

4.Results

4.1 Bulk properties

Mean molecular weights of all three synthesized polyimides were estimated to be ~40000 g/mol. The temperature where 5% weight loss was achieved (T_5) was defined as the onset of thermal decomposition. The temperatures found are in agreement with corresponding data previously published by other groups [57, 96].

Table 1. Glass transition temperatures, thermal decomposition temperatures at 5% weight loss and densities of the polyimides synthesized in this work. Also given are the densities of the simulated polymer systems for both two-chain and five-chain models.

Polymer	T_5 (°C)	ρ_{exp} (kg m^{-3})	ρ_{sim} (kg m^{-3})	
			2 chains	5 chains
6FDA-mPDA	529±5	1456±14	1454±1	1456±1
6FDA-durene	448±4	1333±13	1303±1	1293±1
6FDA-mPDA-durene	507±5	1386±14	1380±1	1354±1

The glass transition temperature found here for 6FDA-mPDA is in good agreement with previously published results [96]. The glass transition temperature of 6FDA-durene could not be determined as it is too close to the onset of degradation. On the other hand, the authors of the aforementioned work report a value of 426 °C [96]. It can be seen in Table 1 that the T_g of the block copolymer is higher than that of 6FDA-mPDA. The increase of T_g with increasing durene content inside a polymer is also comparable with previously published data [96] and can be attributed to the chain stiffness generated by the presence of four methyl groups on the diamine moiety which hinder the rotation of the phenyl ring. The presence of a single glass transition temperature for the block copolyimide indicates that in the case of blocks of M_w = 5000 g/mol there is no phase separation in the material and that the blocks are small enough for it to organise like a statistical random copolymer.

In order to examine any possible variations of the chain dimension with simulation temperature, the square end-to-end distance and square radius of gyration of the polymer chains were evaluated at both elevated (1000K) and room temperature. The obtained values show minor differences for all polyimide models. More specifically, the average square end-to-end distance and radius of gyration of the block copolyimide chains were 56835 and 7305 Å^2 respectively at 1000K whereas at 298K the respective values were 56079 and 7170 Å^2. Analogous trends were detected for the other polyimides.

The density of a simulated system is a fundamental property, since it is governed by the preparation procedure, the accuracy of the force field and other parameters of the model [90]. In addition, many polymer properties such as free volume are directly or indirectly correlated to the density. As it can be seen in table 1, average model densities are all within less than 3% of the corresponding experimental values. Experimental studies in the polyimides of interest have been conducted by other groups for higher chain lengths (average M_w was greater than 140000 in all cases). Reported densities of 6FDA-mPDA lie within the range 1464-1474 kg m^{-3} (average value ~1470 kg m^{-3}) [54, 56, 57, 60, 61], the corresponding ones of 6FDA-durene range from 1327 to 1334 kg m^{-3} (average value ~1332 kg m^3) [59-61, 91, 97], whereas for 6FDA-mPDA/durene density a value of 1385 kg m^{-3} [60, 61] has been found albeit for a *random* copolyimide with 50/50 mPDA/durene molar ratio. Comparison of both our experimental and simulation data with the aforementioned values (taking also into account the differences in average molecular weights) confirms the validity of both approaches. 6FDA-durene is significantly less dense than 6FDA-mPDA as the four methyl diamine groups inhibit chain packing. This is consistent with the higher gas permeabilities of the former. As expected, the density of the 6FDA-mPDA/durene block copolyimide lies between the values of its base homopolyimides.

Table 2 displays the intermolecular potential energies plus their resolutions into the van der Waals and coulombic contributions. The Hildebrand solubility parameter δ [98], also shown in table 2, is given by

$$\delta = \sqrt{\frac{\langle U_{pot}^{inter} \rangle}{\langle V \rangle}} \qquad (3)$$

where $\langle U_{pot}^{inter} \rangle$ is the average intermolecular energy of the system and $\langle V \rangle$ the average volume of the simulation cell.

Table 2. Average volumes of the simulation cells (given in nm^3), intermolecular potential energies (units are kJ mol^{-1} monomer^{-1} and Hildebrand solubility parameters (units are J$^{1/2}$ cm$^{-3/2}$) obtained from the MD simulations of the polyimides under study. The maximum standard errors are ±0.05 nm^3 for the volumes, ±0.08 kJ mole^{-1} molecule^{-1} for the energies and ±0.02 J$^{1/2}$ cm$^{-3/2}$ for the Hildebrand solubility parameters.

Property	6FDA-mPDA		6FDA-durene		6FDA-mPDA/ durene	
No. of atoms	8278	20695	9328	23320	8956	22390
$\langle V \rangle$	103.8	259.3	115.3	290.4	111.1	282.8
$\langle U_{pot}^{inter} \rangle$	-104.6	-105.7	-105.3	-102.9	-104.7	-100.6
$\langle U_{vdw}^{inter} \rangle$	-96.2	-97.0	-98.0	-97.5	-96.6	-93.2
$\langle U_{coul}^{inter} \rangle$	-8.4	-8.7	-7.3	-5.4	-8.1	-7.3
$\langle \delta \rangle$	17.16	17.26	15.47	15.24	16.41	15.84

The average intermolecular potential energies of the models $\langle U_{pot}^{inter} \rangle$ (Table 2) are consistent with other long chain polyimides found in the literature [50, 51, 76, 90]. The major part of the potential energy (more than 90%) originates from the dispersive interactions. Although the dispersive energies for all systems are fairly similar, the simulation box sizes exhibit notable differences implying thus different degree of cohesion among the polyimide samples. This can be easily understood by observing the corresponding Hildebrand solubility parameter values which are directly linked to the cohesive energy density and are also listed in table 1. As expected, the more compact 6FDA-mPDA polyimide bears the highest solubility parameter whereas 6FDA-durene presents the lowest degree of cohesion. All δ values lie within the range of δ=14-28 J$^{1/2}$ cm$^{-3/2}$ which have been estimated for polymers [98]. In general, in order that a polymer is soluble in a solvent, the absolute difference of their corresponding solubility parameters should be as small as possible [96]. Evidently, our simulation values seem compatible with the δ values of solvents generally used for the preparation of fluorinated polyimides such as dichloromethane, tetrahydrofuran and acetone[98,99].

4.2 Structural properties

As already stated in earlier simulation work [100, 101], the indiscriminate intermolecular radial distribution function, $g_{inter}(r)$, can be used to detect whether the atomistic models are actually amorphous or if they show any signs of crystallinity. The $g_{inter}(r)$ calculated over all atoms for all systems are displayed in figure 5.

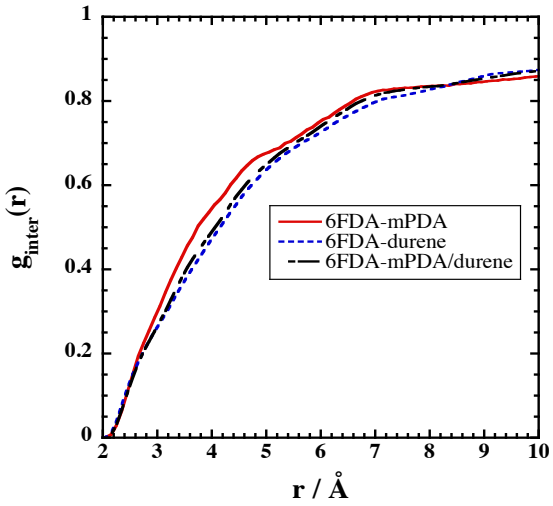

Figure 5. Indiscriminate intermolecular radial distribution functions averaged over all atom pairs for each system under study.

As it can be inferred from figure 5 all polyimide models can be considered to be amorphous since no sign of order is detected in the respective $g_{inter}(r)$ graph in accordance with wide angle X-ray diffraction measurements [54, 102]. The average interchain distance (d-spacing) can also be extracted from the latter by the position of the maximum in the amorphous "halo" in the X-ray diffractogram [51]. A value of 5.33 Å has been reported for 6FDA-mPDA [54] whereas a d-spacing of 6.05 Å is reported for 6FDA-durene [102]. This property can be compared to the average nearest-neighbour intermolecular distance, $r_{0.5}$, arbitrarily defined as $g_{inter}(r_{0.5})$=0.5. As it can be observed in figure 5 the average $r_{0.5}$ of our systems are in the range 3.7 - 4.1 Å and increase in the order 6FDA-durene < 6FDA-mPDA/durene < 6FDA-mPDA. This trend is consistent with the experimental findings.

In order to examine possible preferential structural arrangements between dianhydride and/or diamine fragments in the different polyimides, specific intermolecular radial distribution functions were determined. In the case of diamine-diamine association, diamine rings were represented by pseudoatoms corresponding to the mass unweighted average position of the atoms constituting the ring in order to facilitate comparison between different systems. Moreover, corresponding functions were also determined between dianhydride and diamine fragments. The interactions between the latter have been known to be relevant with regard to charge-transfer complexes (CTC) which are known to occur between alternating electron-rich (diamines) and electron-deficient (dianhydrides) moieties[10, 103, 104]. The corresponding diamine-diamine and anhydride-diamine $g_{inter}(r)$ plots are displayed in figure 6.

Dissimilar behavior is detected among different polyimides. 6FDA-mPDA intermolecular diamine rings are found at short distances from each other as reflected in figure 6a in the peak at approximately 3.5 Å whereas 6FDA-durene diamine pairs do not approach each other at distances closer than 6 Å. 6FDA-mPDA/durene exhibits a stacking behavior that lies between the earlier mentioned profiles. An analogous trend is detected in figure 6b where the diamine-anhydride rings in 6FDA-mPDA system approach each other at shorter distances with respect to 6FDA-durene. Again, the block copolyimide system lies between its base polyimides. Dianhydride-dianhydride interactions are also more prominent in 6FDA-mPDA but in this case the discrepancies between different polyimides are smaller. This can be seen in figure 7 where $g_{inter}(r)$ functions are presented between ketone carbons (C_{ket}) and ketone oxygens (O_{ket}) as well as between the central dianhydride carbon atoms connected to both $-CF_3$ groups (C_{centre}) and ketone oxygens.

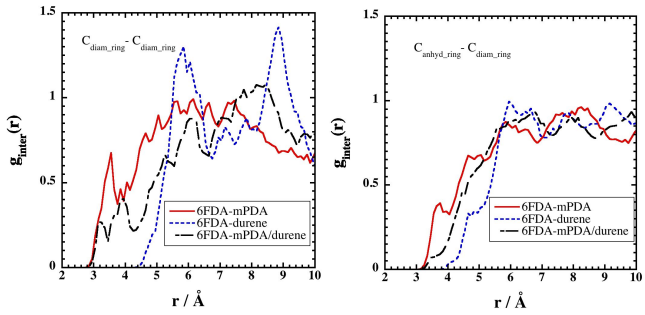

Figure 6. Intermolecular radial distribution functions between a) the diamine rings represented by pseudoatom C_{ring_ring} and b) between the anhydride and diamine rings, the former being represented by pseudoatom C_{anhyd_ring}.

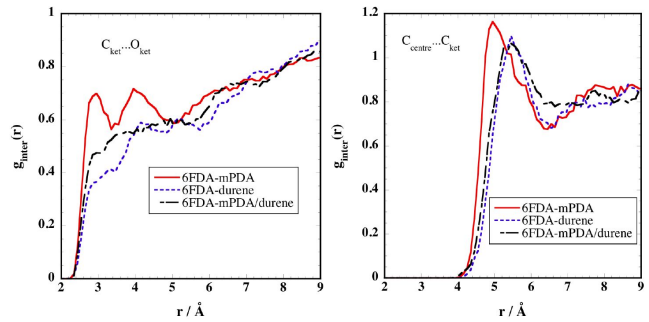

Figure 7. Intermolecular radial pair distribution functions $g_{inter}(r)$ between atoms that belong to dianhydride fragments. Left panel : Ketone carbon (C_{ket})···Ketone oxygen (O_{ket}). Right panel: Central carbon (C_{centre})···Ketone carbon (C_{ket}).

In the case of dianhydride-diamine $g_{inter}(r)$ functions between selected pairs, namely the dianhydride central carbon and diamine carbon as well as between the dianhydride ketone oxygen and diamine carbon (not shown here) exhibit minor differences among the polyimide models.

Similar to the $g_{inter}(r)$ functions, intramolecular radial distribution functions $g_{intra}(r)$ between diamine ring pseudoatoms (not shown) reveal that the nearest distance between two diamine rings in 6FDA-mPDA is around 3.5 Å whereas in 6FDA-durene it nearly doubles. This result further supports the rather poor packing of 6FDA-durene and its extended configuration.

To gain further insight into the distances and orientations between the rings, the least-squares best-fit normal vector to the plane through the atoms constituting each aromatic ring was calculated. The second-order Legendre polynomial functions were then calculated by:

$$P_2(cos\theta) = \frac{3}{2}\langle cos^2\theta\rangle - \frac{1}{2} \qquad (4)$$

where θ is the angle between the vectors normal to the planes of the different rings. $P_2 \cos\theta$ is equal to 1 for a parallel orientation, -0.5 for a perpendicular orientation and 0 for a random orientation. Figure 8 displays the corresponding polynomial functions for the diamine rings.

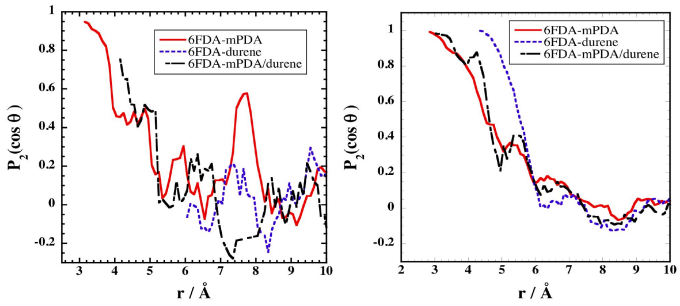

Figure 8. Second order polynomial functions for the intra- (left panel) and intermolecular diamine rings (right panel).

A visual inspection of the intramolecular functions reveals that parallel orientation occurs in 6FDA-mPDA and the block copolyimide system whereas 6FDA-durene diamine rings are randomly orientated probably due to steric reasons. On the contrary, parallel alignment is possible for intermolecular diamine rings at all systems, with the centres of mass of those belonging to 6FDA-durene being further apart than those in the other polyimides. Analogous behaviour is noticed for the corresponding functions of the anhydride rings. The tendency for random orientation among rings at the intramolecular level, inhibits efficient packing of the chains and creates extra space inside the polymer matrix.

4.3 Conformational analyses

In view of the large number of rings in the polymer backbones, the only conformational degrees of freedom come from the rotations around the nitrogen-phenyl bonds of the dianhydride-diamine linkages (C-N-C-C torsional angle) and around the -C(CF_3) linkage of the anhydrides. The probability density distributions for the pivot angle C–C–N–C are shown in figure 9.

We use the convention where the dihedral angle varies from -180 to 180° and τ=0° corresponds to the *trans* conformation. As it can be seen in figure 9, the dianhydride-diamine distribution of 6FDA-mPDA exhibits four well defined peaks at around ±30° and ±148°, which are attributed to the four possible C-C-N-C angles around a dianhydride-diamine linkage. A different profile is observed for 6FDA-durene, as the four peaks mentioned earlier show a tendency to coalesce into two double peaks at around ±122° and ±58°. Although the distribution is slightly broader in this profile, the preferred range of angles is more restricted with respect to 6FDA-mPDA system. This behavior supports the stiffer and more rigid nature of 6FDA-durene system with respect to its 6FDA-mPDA counterpart. As expected, the torsional profile of 6FDA-mPDA/durene exhibits peaks at all τ values already found for its base polyimides.

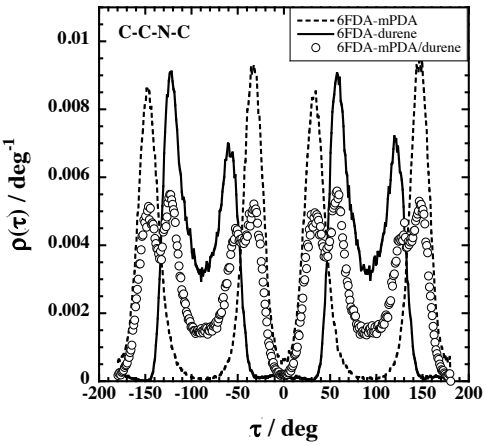

Figure 9. Probability densities for the C - C - N - C dihedral angle for all polyimide models.

4.4 Void space

Free volume is an extremely important property of polymer materials that affects numerous other properties such as viscosity, diffusivity and permeability [25]. Various experimental techniques can be used to determine free volume, namely positron annihilation lifetime spectroscopy (PALS) [27], inverse gas chromatography [105], ^{129}Xe NMR [106] and other probe methods [107, 108]. Free volume fractions (FFV) were estimated using

$$\langle FFV\rangle = \frac{(\langle V\rangle - V_0)}{\langle V\rangle} \qquad (5)$$

where $\langle V\rangle$ is the average volume of the simulation box and V_0 the volume at zero Kelvin (estimated as 1.3 times the van der Waals volume) obtained by Bondi's group contribution method [109]. Application of the above formula yields a value of 0.166 for 6FDA-mPDA, 0.193 for 6FDA-durene and 0.174 for 6FDA-mPDA/durene which compare well with the reported

experimental values 0.156-0.165 for 6FDA-mPDA[57, 60, 96], 0.180-0.183 for 6FDA-durene [97, 110] and 0.177 for 6FDA-mPDA/durene random copolyimide [60, 96]. It should be noted though that this approach involves the consideration of a global factor 1.3 for van der Waals volumes and the approximation of spherical geometries for groups of atoms.

Another way to characterize the void space is through the use of a simple geometric technique referred to as the "phantom sphere approach" which is extensively applied in atomistic simulations [111-114]. The probe accessible volume (PAV) is determined by repeated random insertions of "ghost" probes of preset radius in stored polymer configurations. These probe insertions are performed independently and, therefore, do not "see" the other probes. Standard van der Waals radii are assumed for the polymer atoms: 1.70 Å for C, 1.50 Å for O, 1.20 Å for H, 1.55 Å for N and 1.47 Å for F [98, 109]. An insertion is considered "accepted" or "rejected" according to whether the probe overlaps with any of the polymer atoms. The accessible volume is defined as the total volume of the system multiplied by the percentage of "accepted" insertions. It should be noted here that the PAV is the part of the volume that is accessible to the centre of the probe. Consequently, the actual volume the entire probe can access can not be estimated as the cavities can adopt complicated geometries. In this context, this method can serve as a means of comparing different polyimide systems under the same conditions. The % PAV are given in Table 3 for probe radii ranging from 0 to 2 Å for the two- and five-chain models.

Table 3. Average percentages of probe accessible volume (PAV) for different polyimide models as a function of the probe radius. Maximum errors in the <% PAV> are ±0.04 for probe radii up to 1 Å and ±0.01 for larger probe radii.

System	6FDA-mPDA		6FDA-durene		6FDA-mPDA/durene	
Number of atoms	8278	20695	9328	23320	8956	22390
Probe radius / Å						
0	38.23	38.13	40.84	41.26	39.29	40.39
0.2	27.06	26.84	29.35	29.91	27.87	29.11
0.4	18.39	17.99	20.24	20.78	18.75	20.05
0.6	12.19	11.63	13.37	13.99	12.07	13.37
0.8	7.76	7.26	8.52	9.14	7.47	8.63
1	4.86	4.40	5.28	5.80	4.43	5.39
1.2	2.97	2.59	3.14	3.58	2.52	3.26
1.4	1.79	1.49	1.81	2.13	1.38	1.92
1.6	1.05	0.83	1.0	1.24	0.72	1.10
1.8	0.60	0.45	0.53	0.71	0.35	0.61
2	0.33	0.24	0.26	0.41	0.17	0.35

As expected, the PAV drops systematically with the probe size. It is noteworthy that the closest values to the FFVs estimated via Bondi's approach can be obtained with a probe radius of the order of 0.45 Å. Analogous observations were reported in other simulation studies of bulk polyimides [48, 50]. For the larger size systems, 6FDA-durene exhibits the highest <% PAV>, whereas the smallest amount of void space is found in 6FDA-mPDA for the whole range of probe radii. It should also be noted that the differences in <% PAV> among the polyimide systems tend to decrease with the probe radius. Interestingly, this is not the case for the smaller size systems where the relative order of <% PAV> appears to vary with the probe radius.

In order to obtain a visual perception of the probe insertion process, a representation of the simulation box was drawn and at each successful insertion a black dot was displayed. For a larger number of successful insertions this procedure produced a negative image of the system in 3D perspective [70]. An illustration of the free volume distribution in each polyimide system is provided in figure 10, obtained after performing repeated trial insertions of a 1.9 Å probe which roughly corresponds to a nitrogen-type molecule.

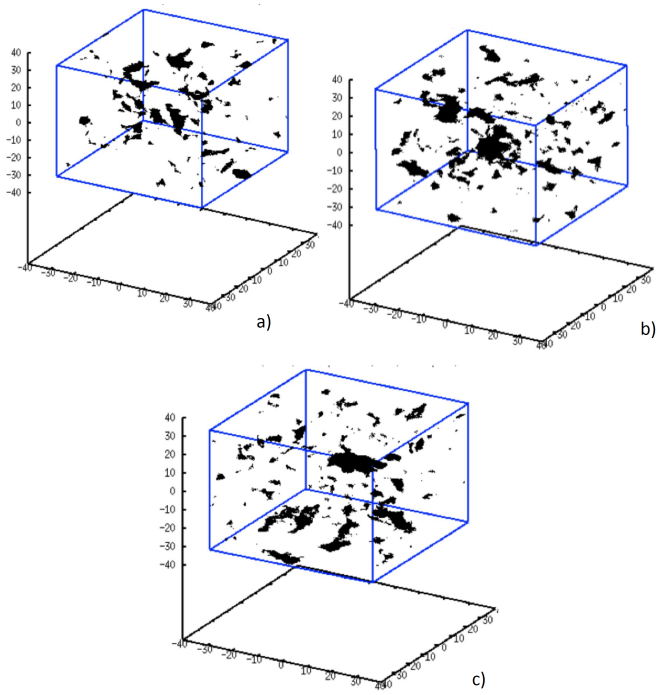

Figure 10. Free volume distribution in a) 6FDA-mPDA, b) 6FDA-durene and c) 6FDA-mPDA/durene 5-chain models obtained after performing trial insertions of a probe of radius 1.9 Å.

A visual inspection of figure 10 reveals that 6FDA-mPDA is characterized by a rather narrow size distribution of free volume elements, the major part of which manifests itself in the form of small to medium hole sizes. On the other hand, the void space is distributed in 6FDA-durene in a more varied manner exhibiting a wide range of hole sizes. This is related to the bulkiness of the methyl groups which inhibit chain packing. The coexistence of both types of diamines (mPDA and durene) in the copolyimide system results in a reorganization of the accessible space.

Conclusions

The purpose of this work was to study the structural characteristics of 6FDA-mPDA/durene copolyimide and its

base homopolyimides 6FDA-mPDA and 6FDA-durene. Given the fact that the dianhydride fragment was common for all polyimides, it was possible to address the influence of different diamines on thermodynamic and static properties at the molecular level. Amorphous models of the three polyimides were generated through the use of a hybrid PMC-MD preparation procedure after optimizing the local energy parameter on short homologues. MD simulations were carried out at 298 K on a series of two- and 5-chain systems. Moreover, the three polyimides of interest were synthesized and were further employed for the preparation of dense flat membranes.

Experimental data of thermal decomposition as well as glass transition temperatures of 6FDA-mPDA and 6FDA-mPDA/durene were found to lie in accordance with pertinent measurements. Moreover, average model densities were found to be in satisfactory agreement with laboratory data of this work and other resources verifying that the preparation method and utilized force field were highly applicable in the systems under study.

Dispersive interactions were found to have the most significant contribution to the cohesive energy. A number of structural properties such as radial distribution functions, torsion angle distributions and ring correlation functions were determined. Intramolecular interactions trigger a more extended configuration for 6FDA-durene. Diamine ring intermolecular interactions in this system are significantly weaker with respect to its 6FDA-mPDA counterpart, implying poorer stacking. This was further supported by the second order Legendre intramolecular polynomial functions between the centroids of the diamine rings which showed a random orientation contrary to those of 6FDA-mPDA and 6FDA-mPDA/durene which are close to being parallel at the shortest intra-ring separations. Moreover, the presence of methyl substituents in 6FDA-durene diamine further inhibits packing due to steric hindrance and restricts rotation around the C-C-N-C angle. All the aforementioned effects are consistent with the lower density, cohesive energy and Hildebrand solubility parameter of 6FDA-durene. The values of the earlier mentioned properties for the block copolyimide lie between those of its base polyimides. Dianhydride-dianhydride interactions show rather small differences among the different polyimide systems with 6FDA-mPDA exhibiting the highest degree of association. The previous findings justify the experimentally determined trend in permeabilities for these polyimides, being 6FDA-mPDA < 6FDA-mPDA/durene < 6FDA-durene.

The average percentage of probe accessible volume in the examined polyimides was determined using a "phantom sphere" approach. Contrary to the other examined properties, the free volume distribution of the examined polyimides was found to be size dependent. A visual inspection of the probe accessible space in the larger size models revealed that 6FDA-durene exhibits a wide distribution of free volume elements contrary to 6FDA-mPDA system where the major part of free volume is characterized by medium sized holes. On the other hand, 6FDA-mPDA/durene presents a broad cavity size distribution due to its less regular structure.

Based on the different structural features of the examined polyimides, a series of membranes with tailored properties targeted for different gas separation applications can be fabricated. The study of the transport of small gases in the studied polyimides is currently in progress and will be the subject of a future publication.

Acknowledgements

We gratefully thank Saudi Aramco for providing a 3-year post-doctoral grant for Ioannis Tanis and Romain Heck as well as for the generous financial assistance for this project. This work was granted access to the HPC resources of CCRT/CINES/IDRIS under the allocation 2012-095053 and 2013-095053 made by GENCI (Grand Equipement National de Calcul Intensif), France. The MUST cluster at the University of Savoie (France) is also acknowledged for the provision of computer time.

Notes and references

[a] Univ. Savoie, LEPMI, F-73000 Chambéry, France, CNRS, LEPMI, F-38000 Grenoble, France, LMOPS – Bât. IUT, Campus de Savoie - Technolac, F-73376 Le Bourget-du-Lac Cedex, France.
E-mails: tanis.ioannis@gmail.com, David.Brown@univ-savoie.fr ; Tel: +33 4 79 75 88 35, Fax: +33 4 79 75 81 64
[b] IMP, UMR 5223, CNRS – Université Claude Bernard Lyon1, Bât. Raulin 5eme, 2 Rue V. Grignard, 69622 Villeurbanne Cedex, France

Electronic Supplementary Information (ESI) available: [Partial charges of the model fragments]. See DOI: 10.1039/b000000x/

1. M. K. Ghosh and K. L. Mittal, *Polyimides: Fundamentals and Applications*, Marcel Dekker Inc, 1996.
2. M. Hegde, U. Lafont, B. Norder, S. J. Picken, E. T. Samulski, M. Rubinstein and T. Dingemans, *Macromolecules*, 2013, **46**, 1492-1503.
3. M. W. Hellums, W. J. Koros, G. R. Husk and D. R. Paul, *J. Membr. Sci.*, 1989, **46**, 93-112.
4. F. P. Laming, *Polym. Eng. Sci.*, 1971, **11**, 421-425.
5. D.-J. Liaw, K.-L. Wang, Y.-C. Huang, K.-R. Lee, J.-Y. Lai and C.-S. Ha, *Prog. Polym. Sci.*, 2012, **37**, 907-974.
6. N. Peng, T.-S. Chung, M. L. Chng and W. Aw, *J. Membr. Sci.*, 2010, **360**, 48-57.
7. C. E. Powell and G. G. Qiao, *J. Membr. Sci.*, 2006, **279**, 1-49.
8. Y. Wang, L. Jiang, T. Matsuura, T. S. Chung and S. H. Goh, *J. Membr. Sci.*, 2008, **318**, 217-226.
9. W. Volksen, in *High Performance Polymers*, ed. P. Hergenrother, Springer Berlin Heidelberg, 1994, vol. 117, pp. 111-164.
10. M. Hasegawa and K. Horie, *Prog. Polym. Sci.*, 2001, **26**, 259-335.
11. X. Zhao, J. Liu, H. Yang, L. Fan and S. Yang, *Eur. Polym. J.*, 2008, **44**, 808-820.
12. S. H. Baek, J.-W. Kang, X. Li, M.-H. Lee and J.-J. Kim, *Opt. Lett.*, 2004, **29**, 301-303.

13. A. Quaranta, A. Vomiero, S. Carturan, G. Maggioni and G. Della Mea, *Synthetic Met.*, 2003, **138**, 275-279.
14. R. A. Synowicki, J. S. Hale and J. A. Woollam, *J. Spacecr. Rockets*, 1993, **30**, 116-119.15. D. Ayala, A. E. Lozano, J. de Abajo, C. García-Perez, J. G. de la Campa, K. V. Peinemann, B. D. Freeman and R. Prabhakar, *J. Membr. Sci.*, 2003, **215**, 61-73.
15. D. Ayala, A. E. Lozano, J. de Abajo, C. García-Perez, J. G. de la Campa, K. V. Peinemann, B. D. Freeman and R. Prabhakar, *J. Membr. Sci.*, 2003, **215**, 61-73.
16. E. Saiz, M. M. Lopez Gonzalez, E. Riande, J. Guzman and V. Compan, *Phys. Chem. Chem. Phys.*, 2003, **5**, 2862-2868.
17. C. Bas, R. Mercier, J. Sanchez-Marcano, S. Neyertz, N. D. Albérola and E. Pinel, *J. Polym. Sci. Part B: Polym. Phys.*, 2005, **43**, 2413-2426.
18. M. R. Coleman and W. J. Koros, *Macromolecules*, 1997, **30**, 6899-6905.
19. L. M. Costello and W. J. Koros, *J. Polym. Sci. Part B: Polym. Phys.*, 1995, **33**, 135-146.
20. C. Hibshman, M. Mager and E. Marand, *J. Membr. Sci.*, 2004, **229**, 73-80.
21. T. H. Kim, W. J. Koros, G. R. Husk and K. C. O'Brien, *J. Membr. Sci.*, 1988, **37**, 45-62.
22. Y.-C. Wang, S.-H. Huang, C.-C. Hu, C.-L. Li, K.-R. Lee, D.-J. Liaw and J.-Y. Lai, *J. Membr. Sci.*, 2005, **248**, 15-25.
23. S. H. Han, H. J. Kwon, K. Y. Kim, J. G. Seong, C. H. Park, S. Kim, C. M. Doherty, A. W. Thornton, A. J. Hill, A. E. Lozano, K. A. Berchtold and Y. M. Lee, *Phys. Chem. Chem. Phys.*, 2012, **14**, 4365-4373.
24. M. L. Cecopieri-Gómez, J. Palacios-Alquisira and J. M. Domínguez, *J. Membr. Sci.*, 2007, **293**, 53-65.
25. Y. P. Yampolskii, I. Pinnau and B. D. Freeman, *Materials Science of Membranes for Gas and Vapour Separation*, John Wiley & Sons Ltd, 2006.
26. J. P. LaFemina, G. Arjavalingam and G. Hougham, *J. Chem. Phys.*, 1989, **90**, 5154-5160.
27. A. Shimazu, T. Miyazaki, S. Katayama and Y. Ito, *J. Polym. Sci. Part B: Polym. Phys.*, 2003, **41**, 308-318.
28. D. Frenkel and B. Smit, *Understanding Molecular Simulation, Second Edition: From Algorithms to Applications (Computational Science)*, Academic Press, 2002.
29. K. Karatasos and I. Tanis, *Macromolecules*, 2011, **44**, 6605-6614.
30. I. Tanis, K. Karatasos, A. N. Assimopoulou and V. P. Papageorgiou, *Phys. Chem. Chem. Phys.*, 2011, **13**, 10808-10817.
31. S. Fotiadou, C. Karageorgaki, K. Chrissopoulou, K. Karatasos, I. Tanis, D. Tragoudaras, B. Frick and S. H. Anastasiadis, *Macromolecules*, 2013, **46**, 2842-2855.
32. O. Hölck, M. Heuchel, M. Böhning and D. Hofmann, *J. Polym. Sci. Part B: Polym. Phys.*, 2008, **46**, 59-71.
33. F. Müller-Plathe, *Acta Polym.*, 1994, **45**, 259-293.
34. D. N. Theodorou and U. W. Suter, *Macromolecules*, 1985, **18**, 1467-1478.
35. R. Khare, M. E. Paulaitis and S. R. Lustig, *Macromolecules*, 1993, **26**, 7203-7209.
36. J. J. de Pablo, M. Laso and U. W. Suter, *J. Chem. Phys.*, 1992, **96**, 2395-2403.
37. V. A. Harmandaris, D. Reith, N. F. A. van der Vegt and K. Kremer, *Macromol. Chem. Physic.*, 2007, **208**, 2109-2120.
38. P. V. Komarov, C. Yu-Tsung, C. Shih-Ming, P. G. Khalatur and P. Reineker, *Macromolecules*, 2007, **40**, 8104-8113.
39. S. V. Lyulin, A. A. Gurtovenko, S. V. Larin, V. M. Nazarychev and A. V. Lyulin, *Macromolecules*, 2013, **46**, 6357-6363.
40. S. V. Lyulin, S. V. Larin, A. A. Gurtovenko, V. M. Nazarychev, S. G. Falkovich, V. E. Yudin, V. M. Svetlichnyi, I. V. Gofman and A. V. Lyulin, *Soft Matter*, 2014, **10**, 1224-1232.
41. M. Minelli, M. G. De Angelis and D. Hofmann, *Fluid Phase Equilibr.*, 2012, **333**, 87-96.
42. R. Pan, W. Zhao, T. Zhou and A. Zhang, *J. Polym. Sci. Part B: Polym. Phys.*, 2010, **48**, 595-599.
43. D. Qi, J. Hinkley and G. He, *Model. Simul. Mater. Sc.* , 2005, **13**, 493.
44. L. Zhang, Y. Xiao, T.-S. Chung and J. Jiang, *Polymer*, 2010, **51**, 4439-4447.
45. S. G. Falkovich, S. V. Lyulin, V. M. Nazarychev, S. V. Larin, A. A. Gurtovenko, N. V. Lukasheva and A. V. Lyulin, *J. Polym. Sci. Part A: Polym. Chem.*, 2014, **52**, 640-646.
46. J. Zhou, X. Zhu, J. Hu, H. Liu, Y. Hu and J. Jiang, *Physical Chemistry Chemical Physics*, 2014, **16**, 6075-6083.
47. M. Heuchela, M. Böhning, O. Hölck, M. R. Siegert and D. Hofmann, *Desalination*, 2006, **199**, 443-444.
48. D. Hofmann, M. Heuchel, Y. Yampolskii, V. Khotimskii and V. Shantarovich, *Macromolecules*, 2002, **35**, 2129-2140.
49. S. Neyertz, D. Brown, A. Douanne, C. Bas and N. D. Albérola, *J. Phys. Chem. B*, 2002, **106**, 4617-4631.
50. S. Pandiyan, D. Brown, N. F. A. van der Vegt and S. Neyertz, *J. Polym. Sci. Part B: Polym. Phys.*, 2009, **47**, 1166-1180.
51. E. Pinel, D. Brown, C. Bas, R. Mercier, N. D. Albérola and S. Neyertz, *Macromolecules*, 2002, **35**, 10198-10209.
52. S. V. Larin, S. G. Falkovich, V. M. Nazarychev, A. A. Gurtovenko, A. V. Lyulin and S. V. Lyulin, *RSC Advances*, 2014, **4**, 830-844.
53. K. Tanaka, M. Okano, H. Toshino, H. Kita and K.-I. Okamoto, *J. Polym. Sci. Part B: Polym. Phys.*, 1992, **30**, 907-914.
54. J.-H. Kim, S.-B. Lee and S. Y. Kim, *J. Appl. Polym. Sci.*, 2000, **77**, 2756-2767.
55. K. Tanaka, Y. Osada, H. Kita and K.-i. Okamoto, *J. Polym. Sci. Part B: Polym. Phys.*, 1995, **33**, 1907-1915.
56. C. Staudt-Bickel and W. J. Koros, *J. Membr. Sci.*, 2000, **170**, 205-214.
57. L. Wang, Y. Cao, M. Zhou, X. Ding, Q. Liu and Q. Yuan, *Polym. Bull.*, 2008, **60**, 137-147.
58. K. Tanaka, A. Taguchi, J. Hao, H. Kita and K. Okamoto, *J. Membr. Sci.*, 1996, **121**, 197-207.
59. W.-H. Lin and T.-S. Chung, *J. Membr. Sci.*, 2001, **186**, 183-193.
60. C. Tai-Shung, L. Wen-Hui and H. V. Rohit, *J Appl Polym Sci*, 2001, **81**, 3552-3564.
61. S.-X. Cheng, T.-S. Chung, R. Wang and R. H. Vora, *J. Appl. Polym. Sci.*, 2003, **90**, 2187-2193.
62. K.-S. Chang, C.-C. Hsiung, C.-C. Lin and K.-L. Tung, *J. Phys. Chem. B*, 2009, **113**, 10159-10169.
63. M. Heuchel and D. Hofmann, *Desalination*, 2002, **144**, 67-72.
64. J. I. McKechnie, D. Brown and J. H. R. Clarke, *Macromolecules*, 1992, **25**, 1562-1567.

65. D. Brown and J. H. R. Clarke, *J. Chem. Phys.*, 1986, **84**, 2858-2865.
66. W. H. Carothers, *Trans. Faraday Soc.*, 1936, **32**, 39-49.
67. J. K. Fink, High performance polymers, 2nd Edition, Elsevier, 2014.
68. H. Ohya, V. Kudryavsev and S. I. Semenova, Polyimide membranes: applications, fabrications and properties, CRC Press, 1997.
69. D. Brown, H. Minoux and B. Maigret, Comput. Phys. Commun., 1997, **103**, 170-186.
70. D. Brown, 2013, Available at http://www.lmops.univ-savoie.fr/brown/gmq_man_V5.pdf.
71. M. Clark, R. D. Cramer and N. Van Opdenbosch, J. Comput. Chem., 1989, **10**, 982-1012.
72. S. Neyertz and D. Brown, Macromolecules, 2013, **46**, 2433-2449.
73. S. Neyertz, A. Douanne and D. Brown, J. Membr. Sci., 2006, **280**, 517-529.
74. S. Neyertz, Macromolecular Theor. Simul., 2007, **16**, 513-524.
75. S. Neyertz, A. Douanne and D. Brown, Macromolecules, 2005, **38**, 10286-10298.
76. S. Neyertz and D. Brown, Macromolecules, 2004, **37**, 10109-10122.
77. S. Neyertz and D. Brown, Macromolecules, 2009, **42**, 8521-8533.
78. S. Neyertz, Soft Mater., 2007, **4**, 15-83.
79. C. L. Chen, H. L. Chen, C. L. Lee and J. H. Shih, Macromolecules, 1994, **27**, 2087-2091.
80. J. H. Shih and C. L. Chen, Macromolecules, 1995, **28**, 4509-4515.
81. P. P. Ewald, Ann. Phys., 1921, **369**, 253-287.
82. K. D. Hammonds and J.-P. Ryckaert, Comput. Phys. Commun., 1991, **62**, 336-351.
83. M. J. T. Frisch, G. W.; Schlegel, H. B.; Scuseria, G. E.; Robb, M. A.; Cheeseman, J. R.; Montgomery, Jr., J. A.; Vreven, T.; Kudin, K. N.; Burant, J. C.; Millam, J. M.; Iyengar, S. S.; Tomasi, J.; Barone, V.; Mennucci, B.; Cossi, M.; Scalmani, G.; Rega, N.; Petersson, G. A.; Nakatsuji, H.; Hada, M.; Ehara, M.; Toyota, K.; Fukuda, R.; Hasegawa, J.; Ishida, M.; Nakajima, T.; Honda, Y.; Kitao, O.; Nakai, H.; Klene, M.; Li, X.; Knox, J. E.; Hratchian, H. P.; Cross, J. B.; Bakken, V.; Adamo, C.; Jaramillo, J.; Gomperts, R.; Stratmann, R. E.; Yazyev, O.; Austin, A. J.; Cammi, R.; Pomelli, C.; Ochterski, J. W.; Ayala, P. Y.; Morokuma, K.; Voth, G. A.; Salvador, P.; Dannenberg, J. J.; Zakrzewski, V. G.; Dapprich, S.; Daniels, A. D.; Strain, M. C.; Farkas, O.; Malick, D. K.; Rabuck, A. D.; Raghavachari, K.; Foresman, J. B.; Ortiz, J. V.; Cui, Q.; Baboul, A. G.; Clifford, S.; Cioslowski, J.; Stefanov, B. B.; Liu, G.; Liashenko, A.; Piskorz, P.; Komaromi, I.; Martin, R. L.; Fox, D. J.; Keith, T.; Al-Laham, M. A.; Peng, C. Y.; Nanayakkara, A.; Challacombe, M.; Gill, P. M. W.; Johnson, B.; Chen, W.; Wong, M. W.; Gonzalez, C.; and Pople, J. A., Gaussian 03, Gaussian Inc., Wallingford, CT, 2004.
84. U. C. Singh and P. A. Kollman, J. Comput. Chem., 1984, **5**, 129-145.
85. D. Feldman, J. Polym. Sci. Part C: Polym. Lett., 1990, **28**, 31-32.
86. S. Neyertz, D. Brown and J. H. R. Clarke, J. Chem. Phys., 1996, **105**, 2076-2088.
87. S. Neyertz and D. Brown, J. Chem. Phys., 2001, **115**, 708-717.
88. D. Brown and S. Neyertz, Mol. Phys., 1995, **84**, 577-595.
89. H. J. C. Berendsen, J. P. M. Postma, W. F. van Gunsteren, A. DiNola and J. R. Haak, J. Chem. Phys., 1984, **81**, 3684-3690.
90. G. Marque, S. Neyertz, J. Verdu, V. Prunier and D. Brown, Macromolecules, 2008, **41**, 3349-3362.
91. W.-H. Lin, R. H. Vora and T.-S. Chung, J. Polym. Sci. Part B: Polym. Phys., 2000, **38**, 2703-2713.
92. W. Smith, Comput. Phys. Commun., 1992, **67**, 392-406.
93. Y. Chen, Q. L. Liu, A. M. Zhu, Q. G. Zhang and J. Y. Wu, J. Membr. Sci., 2010, **348**, 204-212.
94. Y. Jiang, F. T. Willmore, D. Sanders, Z. P. Smith, C. P. Ribeiro, C. M. Doherty, A. Thornton, A. J. Hill, B. D. Freeman and I. C. Sanchez, Polymer, 2011, **52**, 2244-2254.
95. A. W. Humphrey, K. Dalke and K. Schulten, J. Mol. Graphics, 1996, **14**, 33-38.
96. T.-S. Chung, W.-H. Lin and R. H. Vora, J. Appl. Polym. Sci., 2001, **81**, 3552-3564.
97. S. L. Liu, R. Wang, T. S. Chung, M. L. Chng, Y. Liu and R. H. Vora, J. Membr. Sci., 2002, **202**, 165-176.
98. D. W. van Krevelen, Properties of Polymers, Elsevier Science, 1997.
99. R. Recio, L. Palacio, P. Prádanos, A. Hernández, Á. E. Lozano, Á. Marcos, J. G. de la Campa and J. de Abajo, J. Membr. Sci., 2007, **293**, 22-28.
100. J. W. Kang, K. Choi, W. H. Jo and S. L. Hsu, Polymer, 1998, **39**, 7079-7087.
101. R. Zhang and W. L. Mattice, Macromolecules, 1995, **28**, 7454-7460.
102. Y. Xiao, T.-S. Chung, H. M. Guan and M. D. Guiver, J. Membr. Sci., 2007, **302**, 254-264.
103. S. Ando, T. Matsuura and S. Sasaki, Polym J, 1997, **29**, 69-76.
104. F. J. Dinan, W. T. Schwartz, R. A. Wolfe, D. S. Hojnicki, T. S. Clair and J. R. Pratt, J. Polym. Sci. Part A: Polym. Chem., 1992, **30**, 111-118.
105. A. Y. Alentiev, V. P. Shantarovich, T. C. Merkel, V. I. Bondar, B. D. Freeman and Y. P. Yampolskii, Macromolecules, 2002, **35**, 9513-9522.
106. G. Golemme, J. B. Nagy, A. Fonseca, C. Algieri and Y. Yampolskii, Polymer, 2003, **44**, 5039-5045.
107. J. G. Victor and J. M. Torkelson, Macromolecules, 1987, **20**, 2241-2250.
108. Y. P. Yampol'skii, V. P. Shantorovich, F. P. Chernyakovskii, A. I. Kornilov and N. A. Plate, J. Appl. Polym. Sci., 1993, **47**, 85-92.
109. A. Bondi, J. Phys. Chem., 1954, **58**, 929-939.
110. S. L. Liu, R. Wang, Y. Liu, M. L. Chng and T. S. Chung, Polymer, 2001, **42**, 8847-8855.
111. C. Nagel, E. Schmidtke, K. Günther-Schade, D. Hofmann, D. Fritsch, T. Strunskus and F. Faupel, Macromolecules, 2000, **33**, 2242-2248.
112. P. V. K. Pant and R. H. Boyd, Macromolecules, 1993, **26**, 679-686.
113. R. H. Boyd and P. V. K. Pant, Macromolecules, 1991, **24**, 4078-4083.
114. S. Lee and W. L. Mattice, Comput. Theor. Polym. S., 1999, **9**, 57-61.